Acta Biomaterialia 157 (2023) 395–407

Contents lists available at ScienceDirect

Acta Biomaterialia

journal homepage: www.elsevier.com/locate/actbio

Full length article

# Biomimetic camouflaged nanoparticles with selective cellular internalization and migration competences

Carla Jiménez-Jiménez[a,b], Almudena Moreno-Borrallo[a], Bianca Dumontel[a], Miguel Manzano[a,b], María Vallet-Regí[a,b,*]

[a] Department of Chemistry in Pharmaceutical Sciences, School of Pharmacy, Institute Hospital 12 de Octubre (imas12), Universidad Complutense de Madrid, UCM, Madrid 28040, Spain
[b] Networking Research Center on Bioengineering, Biomaterials and Nanomedicine (CIBER-BBN), Madrid 28029, Spain

ARTICLE INFO

*Article history:*
Received 2 September 2022
Revised 8 November 2022
Accepted 29 November 2022
Available online 5 December 2022

*Keywords:*
Nanomedicine
Coating technology
Cell membranes
Nanocarriers for drug delivery

ABSTRACT

In the last few years, nanotechnology has revolutionized the potential treatment of different diseases. However, the use of nanoparticles for drug delivery might be limited by their immune clearance, poor biocompatibility and systemic immunotoxicity. Hypotheses for overcoming rejection from the body and increasing their biocompatibility include coating nanoparticles with cell membranes. Additionally, source cell-specific targeting has been reported when coating nanoparticles with tumor cells membranes. Here we show that coating mesoporous silica nanoparticles with membranes derived from preosteoblastic cells could be employed to develop potential treatments of certain bone diseases. These nanoparticles were selected because of their well-established drug delivery features. On the other hand MC3T3-E1 cells were selected because of their systemic migration capabilities towards bone defects. The coating process was here optimized ensuring their drug loading and delivery features. More importantly, our results demonstrated how camouflaged nanocarriers presented cellular selectivity and migration capability towards the preosteoblastic source cells, which might constitute the inspiration for future bone disease treatments.

**Statement of significance**

This work presents a new nanoparticle formulation for drug delivery able to selectively target certain cells. This approach is based on Mesoporous Silica Nanoparticles coated with cell membranes to overcome the potential rejection from the body and increase their biocompatibility prolonging their circulation time. We have employed membranes derived from preosteoblastic cells for the potential treatment of certain bone diseases. Those cells have shown systemic migration capabilities towards bone defects. The coating process was optimized and their appropriate drug loading and releasing abilities were confirmed. The important novelty of this work is that the camouflaged nanocarriers presented cellular selectivity and migration capability towards the preosteoblastic source cells, which might constitute the inspiration for future bone disease treatments.



## 1. Introduction

Over the last two decades, a wide range of organic and inorganic nanoparticles (NPs) have been extensively explored as diagnostic and therapeutic tools for various biomedical applications [1]. Among them, NPs-based drug delivery systems present several benefits in terms of efficacy and safety. For instance, NPs can improve the stability and solubility of the encapsulated therapeutic agents and limit their rapid clearance and non-specific uptake [2,3]. The design of nanocarriers with desired circulation and targeting capabilities require the development of finely tailored functionalization strategies, able to address the high complexity of biological systems. In this sense, emerging approaches involve coating synthetic NPs with biologically-derived materials, like extracellular vesicles derived from mammalian cells [4] and bacteria [5] or nat-

* Corresponding author at: Department of Chemistry in Pharmaceutical Sciences, School of Pharmacy, Institute Hospital 12 de Octubre (imas12), Universidad Complutense de Madrid, UCM, Madrid 28040, Spain.
*E-mail address:* vallet@ucm.es (M. Vallet-Regí).

https://doi.org/10.1016/j.actbio.2022.11.059

ural cell membranes [6], leading to the formulation of bioinspired NPs.

Cell membranes are naturally designed for optimal interaction with the physiological environment and show several valuable properties for drug delivery applications, like high biocompatibility [7] and inherent homo- or heterotypic adhesion properties, depending on the cell source [8]. These unique features are finely regulated by the specific lipid composition [9], antigenic profile [10] and other constituents of the cell membranes, which are object of continuous study. The increasing understanding of specific membrane factors has led to a variety of functionalization strategies of the surface of nanoparticles that attempt to artificially mimic the cell surface. Examples of this approach include coating NPs with synthetic [11,12] or natural biomolecules [13]. However, these approaches require demanding compositional studies and complex multi-functionalization processes. Coating NPs with natural cell membranes, on the other hand, would allow to transfer all their bioactive functions in a one-step solution [8]. Thanks to this simple top-down approach, cell membrane-coated NPs could combine the flexibility and scalability of synthetic nanocarriers with the intrinsic biointerfacing capabilities of biologically-derived materials.

Cell membrane-coating nanotechnology was originally applied to promote the *in vivo* systemic circulation of NPs by coating poly(lactic-co-glycolic acid) (PLGA) NPs with red blood cell (RBC) membranes [14]. Erythrocytes are naturally endowed with long *in vivo* survival [15] and this feature was efficiently translocated to the PLGA NPs. In fact, when injected into mice, the RBC membrane-coated NPs exhibited a longer circulation half-life with respect to their PEG-coated counterparts, indicating the potential of using this biological material [14]. Since then, RBC membranes [16,17] and membranes derived from other cell sources, like leukocytes [18], macrophages [19], platelets [20–22], mesenchymal stem cells [23–25] and cancerous cells [8,26], were used to coat different types of particles. In all cases, these hybrid formulations showed low immune recognition together with immune-modulatory capabilities, which made them promising candidates for the development of effective drug delivery systems [6,27,28]. Additionally, the ability of cancerous cell and immune cell membrane coatings to target the source cells or inflammation sites, respectively, has been extensively reported [29,30]. The specific uptake and the ability to cross a pulmonary cell monolayer of acetalated dextran NPs coated with pulmonary epithelial cell membranes was also recently demonstrated [31]. The study reported the superior specificity and transport of membrane-coated NPs with respect to lipid- and polymer-coated NPs, indicating the presence of specific cell type molecules as the main driving force behind this enhancement [31].

To date, cell membrane-coated NPs have been intensively investigated for their application in the treatment of various diseases, such as cancer [32,33], infections [34,35] and neurodegenerative diseases [36], and the high versatility of this nanotechnology leaves open the possibility of further applications. The opportune selection of the cell source would allow the specific delivery of membrane-coated NPs to different physiological or pathological sites, thus expanding the range of action of this technology. Among others, bone diseases, such as osteoporosis, bone cancer or bone infection, are becoming a major issue because of the progressive ageing in modern societies [37]. Some current treatments present many inconveniences that could lead to even worst consequences, such as the side effects from some anti-osteoporotic treatments due to the high doses needed to confront their poor bioavailability; the lack of tumor selectivity of conventional anticancer drugs; or the massive and inappropriate use of antibiotics that leads to the increment of drug-resistant bacteria. A potential solution could be the encapsulation and selective delivery of certain therapeutic agents to the specific bone diseased tissues. In this sense, nanoparticles could be the ideal transportation vector because of their versatility and specificity [38].

In this work, we propose the use of membranes derived from the MC3T3-E1 preosteoblastic cell line for the development of biomimetic coated NPs targeted towards bone diseases. Indeed, bone infection, bone cancer and osteoporosis are pressing pathological conditions and their treatment with NPs-based technologies is widely investigated [39,40]. To our knowledge, no nanocarriers formulated with a cell membrane-coating strategy have been proposed for the targeting of such diseases and this approach could be exploited for the development of future therapeutic options. Osteoblast precursors are known to be involved in embryonic bone formation and bone repair [41]. While differentiated osteoblasts require an extracellular matrix of certain rigidity to migrate, osteoblast precursor cells migrate towards bone tissue through the blood vessels [42]. By coating the NPs with cell membranes from osteoblast precursors we aimed to exploit and transfer these valuable innate capabilities to our nanosystem. Specifically, murine MC3T3-E1 osteoprogenitor cells are one of the most commonly used models for the *in vitro* evaluation of therapeutic agents for the treatment of osteoporotic disease [43]. Moreover, when administered *in vivo*, MC3T3-E1 cells have shown systemic migration capability toward bone defects and enhancement of bone healing [44], which make them an interesting source for membrane harvesting and development of bioinspired coating.

Mesoporous silica nanoparticles (MSNs) were selected as the synthetic core, thanks to their well-established drug delivery properties [45–47]. MSNs are highly biocompatible and biodegradable [48] and possess a high loading capacity due to their large pore volume and surface area and adjustable pore distribution [49]. MSNs were functionalized with two types of aminosilanes to optimize the coating procedure, and both nanocarriers were tested in combination with different amounts of preosteoblast cell membranes. Their effect in cargo release was evaluated as a key parameter for optimization. The biocompatibility and the biointerfacing capabilities of the optimized membrane-coated MSNs were evaluated *in vitro* on different cell lines. As a proof of concept of the efficacy of this biomimetic coating approach, the effect of the cell membrane coating on the selectivity and migration capability toward preosteoblastic source cells was carefully assessed.

## 2. Experimental section

### 2.1. Materials

Cetyltrimethylammonium bromide (CTAB), tetraethyl orthosilicate (TEOS), [3-(2-Aminoethylamino)propyl]trimethoxysilane (DAMO), rhodamine B isothiocyanate, fluorescein isothiocyanate (FITC), calcein, sodium dodecyl sulfate (SDS) and ethylenediaminetetraacetic acid (EDTA) were purchased from Sigma-Aldrich. 3-Aminopropyltriethoxysilane (APTES) was purchased from ABCR GmbH & Co. KG. Phosphate-buffered saline (PBS) solution was bought from GIBCO. UltraCruz® Protease Inhibitor Cocktail Tablet EDTA-free was purchased from Santa Cruz Biotechnology. Dimethyl sulfoxide (DMSO) was acquired from PanReac. The deionized water was purified using a Milli-Q Advantage A-10 purification system (Millipore Corporation) to a final resistivity of 18.2 MΩ cm. All other chemicals (toluene, ammonium nitrate, acetone, absolute ethanol, phosphotungstic acid, sodium hydroxide, etc.) were obtained from Sigma-Aldrich and used as received.

Reagents for *in vitro* assays were as follows: sucrose, triton X-100, bovine serum albumin (BSA), paraformaldehyde, Thiazolyl Blue Tetrazolium Bromide, Trypan Blue (TB), propidium iodide (PI), phalloidin-Atto 565, fluoroshieldTM with DAPI and Dulbecco's Modified Eagle Medium: Nutrient Mixture F-12 (DMEM/F12) from

Sigma-Aldrich; Alpha modified Eagle's medium ($\alpha$-MEM), Dulbecco's Modified Eagle Medium (DMEM), fetal bovine serum (FBS) and L-glutamine from Gibco; penicillin/streptomycin (13-0050) from ZellShield.

### 2.2. Synthesis and surface functionalization of mesoporous silica nanoparticles

Mesoporous silica nanoparticles were synthesized according to a modification of the Stöber method [50] using CTAB as structure directing agent and TEOS as silica precursor. Briefly, 1 g of CTAB was dissolved in 480 mL of deionized water and 3.5 mL of NaOH 2 M in a round-bottom flask. The mixture was kept at 80 °C for 30 min under moderate magnetic stirring and then 5 mL of TEOS were added dropwise using an automated syringe pump at a flow rate of 0.33 mL/min. The synthesis mixture was maintained at 80 °C under continuous magnetic stirring for 2 h and then washed once with water and twice with ethanol and centrifuged at 17,000 g for 15 min. The final product was dried at 70 °C overnight.

Rhodamine B-labeled or fluorescein-labeled MSNs were produced following the same procedure but adding the dye solution to the TEOS at the beginning of the reaction. To allow the dye incorporation in the silica structure, Rhodamine-B isothiocyanate or FITC (1 mg) were previously reacted with 2.2 µL of APTES in 100 µL of ethanol for 2 h and then mixed with TEOS right before the injection.

The MSNs surface was functionalized with amino groups using DAMO or APTES. Two portions of 0.5 g of MSNs were dried under vacuum at room temperature for 5 h, purged with $N_2$ and then redispersed in dry toluene by magnetic stirring. Then, a solution of dry toluene containing 60 µL of DAMO or APTES (*i.e., ca.* 10% wt with respect to the MSNs) was added dropwise. The DAMO functionalization was carried out overnight at 110 °C under inert atmosphere. Then, the nanoparticles were centrifuged at 17,000 g for 15 min and washed with toluene, acetone and twice with ethanol. For APTES functionalization, the mixture was kept overnight at 80 °C under continuous stirring and inert atmosphere and then the nanoparticles were recovered and washed with toluene, ethanol, water and twice with ethanol.

Finally, the CTAB was removed by ionic exchange using a solution of ammonium nitrate ($NH_4NO_3$, 0.32 M in 95% ethanol). The functionalized MSNs were redispersed in the extracting solution (350 mL per 1.4 g of MSNs) and the mixture was refluxed at 80 °C overnight under continuous magnetic strirring. Then the nanoparticles were recovered by centrifugation and washed once with water and twice with ethanol and centrifuged at 17,000 g for 15 min. The same extracting procedure was repeated for 2 h and the final product was washed and dried at 70 °C overnight.

### 2.3. Physico-chemical characterization of MSNs

Nitrogen adsorption measurements were performed to determine the surface area and pore size value, using a Micromeritics ASAP 2010 sorptometer. Brunauer-Emmett-Teller (BET) method was applied to the linear part of the isotherm to calculate the MSNs surface area [51] while Barrett–Joyner–Halenda (BJH) method was applied to the desorption branch to determine the pore size distribution [52]. Mesopore diameter was estimated from the maximum of the pore size adsorption distribution curve.

The mesostructured order of the pores was also confirmed by X-ray diffraction (XRD) using a Philips X-Pert MPD diffractometer equipped with Cu K$\alpha$ radiation.

The surface composition of MSNs was analyzed by Fourier Transformed Infrared (FT-IR) spectroscopy by a Nicolet Nexus spectrometer (Thermo Fisher Scientific).

The MSNs size, shape and morphology were analyzed through transmission electron microscopy (TEM) with a JEOL JEM 1400 electron microscope operated at 200 kV and equipped with a charge-coupled device (CCD) camera (KeenView Camera). The samples were dispersed in HPLC grade water, deposited on holey carbon-coated copper grids and stained with a 1% phosphotungstic acid solution in water.

The hydrodynamic size distribution and $\zeta$-potential of MSNs in water were measured with a Zetasizer Nano ZS (Malvern Instruments) equipped with a 633 nm laser.

The percentage of organic matter in the samples was quantified through thermogravimetry and differential thermal analysis (TGA/DTA) with a PerkinElmer Pyris Diamond TG/DTA analyzer. The analyses were carried out under air flow with a heating rate of 5 °C/min from room temperature to 600 °C and a complementary oxygen flow.

### 2.4. Cell membrane harvesting

MC3T3-E1 cells (subclone 4, CRL-2593, ATCC) were cultured in $\alpha$-MEM supplemented with 10% FBS, 2 mM L-glutamine and 1% penicillin-streptomycin at 37 °C under atmosphere conditions of 5% $CO_2$ and 95% humidity. Then, to harvest the membranes, cells were detached with 2 mM EDTA in PBS, washed with PBS three times and centrifuged at 800 g for 5 min. Cells were then resuspended in a hypotonic lysis buffer with the following composition: 20 mM tris(hydroxymethyl)aminomethane (Tris)-HCl, 10 mM KCl, 2 mM $MgCl_2$ and 1 EDTA-free protease inhibitor cocktail tablet in 10 mL of $H_2O$. Cells were mechanically disrupted using a dounce homogenizer for 20 passes and the resulting solution was centrifuged at 3200 g for 5 min. The supernatant was recovered while the pellet was resuspended in the hypotonic lysis buffer, homogenized and centrifuged a second time. The two supernatants were reunited and centrifuged at 20,000 g for 30 min using a XL-90 Ultracentrifuge equipped with 70Ti fixed-angle Rotor (Beckman Coulter). The pellet was then discarded and the supernatant was ultracentrifuged again at 80,000 g for 1.5 h to finally isolate the cell membranes. The membrane-containing pellet was resuspended in 10 mM Tris-HCl, 1 mM EDTA in PBS buffer and stored at 4 °C.

### 2.5. MSNs coating with cell membranes

The MSNs functionalized with DAMO (MSNs-NH-$NH_2$) or APTES (MSNs-$NH_2$) were coated with MC3T3-E1 cell membranes by co-incubating the two components under vigorous orbital shaking (200 rpm) at 37 °C for 1.5 h. In detail, 10 mg of MSNs were redispersed in 2 mL of deionized water and mixed with 2 mL of PBS containing the harvested cell membranes. To optimize the coating procedure, a range of different amounts of cell membranes (measured in millions of source cells) were explored, namely 1, 4, 7, 14 and 21 million of MC3T3-E1 cells. After the incubation, the membrane-coated MSNs were recovered by centrifugation at 13,000 g for 15 min and redispersed in a 1:1 PBS:$H_2O$ solution by sonicating at room temperature for 30 min. The temperature of the ultrasonic bath was constantly monitored, avoiding any significant increase to prevent sample damage. A second centrifugation step was performed and the final product was stored at 4 °C.

### 2.6. Calcein loading and release assay

Calcein was used as cargo model to evaluate the loading efficiency and the release from membrane-coated MSNs because of its inability to cross cellular membranes. Before the cell-membrane coating procedure, MSNs functionalized with DAMO (MSNs-NH-$NH_2$) or APTES (MSNs-$NH_2$) were loaded by incubating

the nanoparticles with calcein at a 10:1 ratio (mg MSNs:mg calcein) in water. The solution was kept under vigorous stirring at room temperature overnight and then centrifuged at 8,700 g for 15 min and thoroughly washed with PBS and water to remove unloaded calcein. The loaded MSNs (MSNs@CAL) were then coated with different ratios of MC3T3-E1 cell membranes as previously described.

The release assay was performed in 24-transwell plates, by placing 1 mg of membrane-coated MSNs@CAL dispersed in 100 µL of PBS (pH = 7.4) in the transwell permeable support and 600 µL of PBS in the well below. The plate was placed in an orbital shaker at 37 °C and 100 rpm. At each time point, the solution in the wells was collected and analyzed by measuring fluorescence with a Biotek Synergy 4 microplate reader (excitation/emission: 470/509 nm) to quantify the released calcein and the collected solution was replaced with fresh PBS. After 72 h, the PBS was replaced by the same volume of a sodium dodecyl sulphate (SDS) solution (0.5% in PBS), which is a detergent known for disrupting the cell membrane-coating, consequently triggering the calcein release. The assay was carried out for 7 additional days, collecting the medium every 3 h and replacing it with 0.5% SDS in PBS. All the samples were analyzed in triplicate and samples without the addition of 0.5% SDS were also analyzed as negative control.

### 2.7. In vitro *cell assays*

#### 2.7.1. Cell culture

A murine pre-osteoblastic cell line (MC3T3-E1) was cultured as mentioned above. HeLa cells were maintained in DMEM and HGUE-GB-39 cells were cultured in DMEM/F12. Both culture media were supplemented with 10% FBS, 2 mM L-glutamine and 1% penicillin/streptomycin at 37 °C under atmosphere conditions of 95% humidity and 5% $CO_2$. To perform the *in vitro* cellular assays, the cells were seeded and cultured for 24 h before being exposed to the different nanosystems.

#### 2.7.2. Cell internalization and confocal microscopy assay

For the internalization test, MC3T3-E1, HeLa and HGUE-GB-39 cells were seeded and cultured in 6-well plates ($1 \times 10^6$ cell/well) in the presence of the different concentrations of coated and uncoated fluorescein-labeled MSNs (1, 2.5, 5, 10, 25, 50 or 75 µg/mL of MSNs or MSNs@7M MC3T3-E1) for 3 h at 37 °C and 5% $CO_2$. The 7 M coated MSNs were selected based on the results observed in the optimization of the membrane-coating procedure, as described in detail in the results section. For the control experiments, the cells were incubated without nanoparticles. Then, the cells were trypsinized and centrifuged at 966 g for 5 min at 15 °C. The cell pellet was then resuspended in 250 µL of PBS and 50 µL of TB in the absence of light and kept on ice until measurement. TB (0.4%) was used to quench the fluorescence of non-internalized MSNs that might be attached to the outer cell membrane, since TB cannot enter the membranes of live cells. The analysis of membrane-coated and uncoated fluorescein nanoparticles internalized by live cells was performed on a FACSCalibur flow cytometer (Becton Dickinson). The percentage of cells that had internalized the nanoparticles was quantified as the number of fluorescein-positive cells divided by the number of live cells. Untreated cells were used as controls. Data are mean ± SD of three independent experiments.

For the confocal microscopy assay, the cells were treated with a single representative concentration of fluorescein-labeled MSNs or MSNs@7M MC3T3-E1 for 3 h. The cells were then washed with PBS 1X and fixed with 4% paraformaldehyde in PBS (w/v) with 1% sucrose at 37 °C for 20 min. After this time, the cells were again washed with PBS 1X and permeabilized with Triton X-100 at 4 °C for 5 min. Cell membranes and nuclei were then stained with phalloidin (10 µL in 1 mL PBS 1X) and DAPI (3 µM in PBS 1X) at 37 °C for 20 min and 5 min, respectively. Finally, the images were collected with an FV1200 laser scanning microscope (Olympus).

#### 2.7.3. Cell proliferation assay

For the cell cytotoxicity assay, MC3T3-E1, HeLa and HGUE-GB-39 cells were seeded on 96-well plates 24 h prior to the experiment (10,000 cells/well). After this time, the cells were exposed to different concentrations of nanoparticles (1, 2.5, 5, 10, 25, 50 or 75 µg/mL of MSNs or MSNs@7M MC3T3-E1) for 3 h at 37 °C. The cells were then washed with PBS several times and measured. Cell viability was measured using Thiazolyl Blue Tetrazolium Bromide according to the manufacturer's instructions. In this method, live cells reduce XTT tetrazolium by an active mitochondrial dehydrogenase enzyme, which produces insoluble blue formazan crystals that can be quantified colorimetrically. Therefore, 20 µl of 3-(4,5-dimethyl-thiazol-2-yl)2,5-diphenyl tetrazolium bromide (MTT, 5 mg/mL) were added to each well and incubated for 4 h at 37 °C. After this time, the MTT solution was removed and 100 µL of DMSO were added to dissolve the crystals. Subsequently, a microplate reader (Sinergy 4, BioTek, USA) was used to measure the absorbance at 570 nm. Untreated cells were used as controls. Data are mean ± SD of three independent experiments.

#### 2.7.4. Intracellular reactive oxygen-species (ROS) production

MC3T3-E1 cells were seeded in 6-well plates ($1 \times 10^6$ cell/well) and exposed to the nanosystems at different concentrations (5, 10, 25 µg/mL of MSNs or MSNs@7M MC3T3-E1) for 3 h at 37 °C. After this time, in order to determine the production of ROS, the cells were harvested and incubated with 100 mM 2',7'-dichlorofluorescein diacetate (DCFH/DA) at 37 °C for 30 min. DCF fluorescence was measured using a FACSCalibur flow cytometer (Becton Dickinson). Untreated cells were used as controls. Data are mean ± SD of three independent experiments.

#### 2.7.5. Cell cycle analysis

After exposure of MSNs in MC3T3-E1 cells in the same way as the ROS, the cells were trypsinized and collected in PBS. Then, 700 µL of ice-cold 100% ethanol were added dropwise while vortexing. The samples were left overnight at 4 °C. Then, 700 µL of PBS were added to all samples and centrifuged at 1,315 g for 5 min. After this time, the cells were washed again with PBS and a mixture containing 50 µg/mL PI and 100 µg/mL RNase in PBS was added to the pellets. After this step, the samples were incubated under orbital shaking for 3 h at room temperature and in the absence of light. Finally, PI fluorescence analysis was performed in a flow cytometer (FACSCalibur). Data represent the mean ± SD of three independent cultures.

#### 2.7.6. Cell migration assay

To study the migration ability of coated and uncoated MSNs in different cell lines, inserts with 3 µm pore size polycarbonate membranes (Costar) were used in 12-well plates. 1 mg of FITC-labelled MSNs or MSNs@7M MC3T3-E1 in 500 µl of culture medium was added to the inserts. Similarly, 20,000 cells/mL of each cell line was added to the well below. The migration medium was used as a negative control. After 24 h, the non-migrating MSNs were removed from the top and bottom of the polycarbonate membrane and quantified on a Biotek Synergy 4 microplate reader (excitation/emission: 490/520 nm). To quantify the MSNs retained inside the membrane, the polycarbonate membrane was dissolved with DMSO and the retained MSNs were evaluated in the same way as in the two previous cases. Nuclei of cells adhering to the well were stained with DAPI. A fluorescence microscope with a 20x magnification objective was used to observe the migrating MSNs internalized by the cells (three individual fields per well).

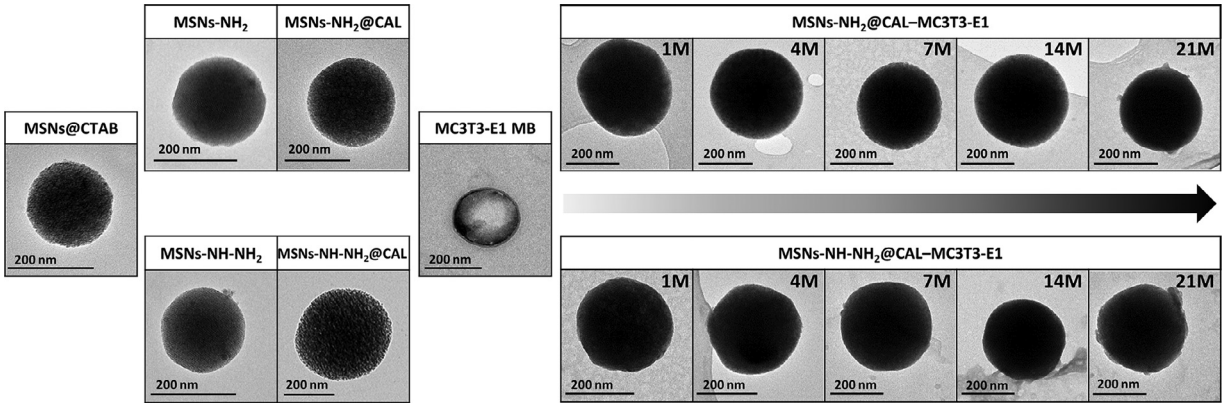


**Fig. 1.** Left: TEM micrographs of MSNs as-produced (MSNs@CTAB), after modifying them with APTES (MSNs-$NH_2$) or DAMO (MSNs-NH-$NH_2$), and after loading them with calcein (MSNs-$NH_2$@CAL and MSNs-NH-$NH_2$@CAL); Centre: cell membranes harvested from pre-osteoblastic MC3T3-E1 cells (MC3T3-E1 MB); Right: MSNs coated with MC3T3-E1 cell membranes (MSNs-$NH_2$@CAL–MC3T3-E1 and MSNs-NH-$NH_2$@CAL–MC3T3-E1) at different concentrations, namely 1, 4, 7, 14 and 21 million (M) of source cells per 10 mg of MSNs. All samples were stained with a 1% phosphotungstic acid (PTA) solution in water.

### 2.8. Statistical analysis

*In vitro* data are expressed as mean ± SD. Unpaired two-tailed Student's t-test were used to determine the statistical significance. $P < 0.05$ was considered significant. Statistical analyses for cellular results were performed using the program Graphpad Prism (Graphpad software). Confocal images were evaluated using the Fiji software (Image J).

## 3. Results and discussion

### 3.1. Synthesis of MSNs and chemical functionalization with aminosilanes

MSNs with spherical shape and size of about 200–300 nm were synthesized through a modification of the Stöber method [50]. The outer surface was then functionalized with amino groups by post-synthesis grafting of aminosilanes functionalizing agents. In particular, two aminosilanes were used, *i.e.* (3-aminopropyl)triethoxysilane (APTES) and N-(2-aminoethyl)-3-aminopropyltrimethoxysilane (DAMO), with one and two amino groups, respectively. The purpose of this functionalization step was to obtain MSNs with a positive surface charge to favor their interaction with negatively charged cell membranes.

The TEM micrographs (Fig. 1) confirmed the expected spherical shape, structure and size of MSNs, which were maintained after the chemical functionalization with APTES (MSNs-$NH_2$) and DAMO (MSNs-NH-$NH_2$). The hydrodynamic size, measured by DLS technique, further confirmed the homogeneity of the samples, which presented narrow monomodal distributions centered at a diameter of around 260 nm (Table 1).

Concerning the surface charge, unmodified MSNs (MSNs@CTAB) presented a negative surface charge ascribable to the presence of silanol groups, while both MSNs-$NH_2$ and MSNs-NH-$NH_2$ showed a positive charge, suggesting the success of functionalization processes (Table 1). Specifically, MSNs functionalized with DAMO exhibit a higher Z-Potential value than those functionalized with APTES, due to the large number of amino groups on the former nanoparticles. The presence of the amino groups was further confirmed by FTIR spectroscopy, accounting the appearance of -$NH_2$ and -NH- vibration bands together with bands corresponding to -$CH_2$- and -$CH_3$ groups, which are also present in the aminosilanes. FTIR analysis also confirmed the successful removal of CTAB, the surfactant used as template to obtain the ordered mesopore structure. This is evidenced by the reduction of the vibration bands intensity from the -$CH_x$ alkyl groups (see Supporting Information Fig. S1A,B).

The mesoporous structure of the two functionalized samples after the CTAB removal was analyzed through $N_2$ adsorption and X-ray diffraction. The results were in good agreement with those reported in literature for MSNs [53–55] and confirmed the mesoporosity of the obtained materials as well as the expected hexagonal symmetry as presented in detail in Fig. S2.

### 3.2. MSNs coating with pre-osteoblastic MC3T3-E1 cell membranes

Cell membranes (MC3T3-E1 MB) were harvested from pre-osteoblastic MC3T3-E1 cells through a lysis and ultracentrifugation protocol resulting in a mixture of disordered or spherically organized fragments, as shown in Fig. 1. As expected, MC3T3-E1 MB presented a negative Z-potential value (Table 1), typical of cell membranes and related to their composition of phospholipids, proteins, and polysaccharide conjugates [56,57].

Amino-functionalized MSNs were loaded with a calcein fluorescent probe before coating them with cell membranes. As shown by TEM and DLS measurements (Fig. 1 and Table 1), both MSNs-$NH_2$@CAL and MSNs-NH-$NH_2$@CAL presented analogous results to their corresponding unloaded counterparts, showing that the process of loading did not affect the size, structure and surface charge of MSNs. The presence of calcein was confirmed by thermogravimetric analyses that detected an increase in the percentage of organic matter in both MSNs-$NH_2$@CAL and MSNs-NH-$NH_2$@CAL samples with respect to the unloaded functionalized nanoparticles (Table 1). Also, FTIR spectroscopy confirmed the calcein loading, accounting to the appearance of a vibration band at *ca.* 1800 $cm^{-1}$ corresponding to calcein C=O groups (MSNs@CAL in Fig. S1C,D).

Different amounts of MC3T3-E1 cell membranes, quantified in millions of source cells, were then combined with APTES or DAMO functionalized MSNs in order to explore the optimal conditions for MSNs coating. The obtained samples were fully characterized evidencing the interactions between preosteoblastic cell membranes and amino-functionalized MSNs. TEM analysis, showed in Fig. 1, revealed the presence of organic material coating the surface of MSNs functionalized with both APTES (MSNs-$NH_2$@CAL–MC3T3-E1) and DAMO (MSNs-NH-$NH_2$@CAL–MC3T3-E1). The staining with phosphotungstic acid allowed the visualization of a dense and homogenous coating in all samples, clearly indicated by the difference in contrast of coated MSNs which appear darker than the uncoated ones. In fact, while the mesoporous structure is clearly visi-

**Table 1**
Mean hydrodynamic sizes, Z-Potential values and relative percentages of organic matter of: cell membranes harvested from pre-osteoblastic MC3T3-E1 cells (MC3T3-E1 MB); MSNs after the synthesis (MSNs@CTAB), functionalization with APTES (MSNs-$NH_2$) or DAMO (MSNs-NH-$NH_2$) and loading with calcein (MSNs-$NH_2$@CAL and MSNs-NH-$NH_2$@CAL); MSNs coated with MC3T3-E1 cell membranes (MSNs-$NH_2$@CAL–MC3T3-E1 and MSNs-NH-$NH_2$@CAL–MC3T3-E1) at different concentrations, namely 1, 4, 7, 14 and 21 million (M) of source cell per 10 mg of MSNs. Hydrodynamic size distributions and Z-potentials were measured in water. The percentages of organic matter are expressed as percentage increase with respect to the MSNs-$NH_2$ or MSNs-NH-$NH_2$ functionalized nanoparticles, indicated as 0 values.

| MSNs-$NH_2$ | | | | | | | | | |
|---|---|---|---|---|---|---|---|---|---|
| | MC3T3-E1 MB | MSNs @CTAB | MSNs -$NH_2$ | MSNs @CAL | MSNs@CAL-MC3T3-E1 | | | | |
| | | | | | 1 M | 4 M | 7 M | 14 M | 21 M |
| **DLS [nm]** | 122 | 268 | 265 | 296 | 231 | 234 | 261 | 295 | 215 |
| **Z-Potential [mV]** | −13.6 | −12.9 | +7.21 | +7.21 | −2.46 | −5.27 | −13.7 | −19.5 | −16.5 |
| **Org. matter [%]** | - | - | 0 | 8.1 | 38.0 | 48.1 | 21.3 | 18.1 | 22.5 |
| MSNs-NH-$NH_2$ | | | | | | | | | |
| | MC3T3-E1 MB | MSNs @CTAB | MSNs -NH-$NH_2$ | MSNs @CAL | MSNs@CAL-MC3T3-E1 | | | | |
| | | | | | 1 M | 4 M | 7 M | 14 M | 21 M |
| **DLS [nm]** | 122 | 268 | 269 | 251 | 279 | 268 | 259 | 296 | 231 |
| **Z-Potential [mV]** | −13.6 | −12.9 | +15.6 | +15.6 | +6.71 | +5.47 | +3.68 | +1.81 | +9.06 |
| **Org. matter [%]** | - | - | 0 | 25.7 | 51.7 | 49.9 | 33.9 | 39.1 | 45.2 |

ble in MSNs-$NH_2$ and MSNs-NH-$NH_2$, this is masked after the addition of cell membranes, suggesting the presence of a coating layer shielding the silica core [58]. In MSNs-$NH_2$@CAL–21M MC3T3-E1 and MSNs-NH-$NH_2$@CAL–21M MC3T3-E1 samples, small fragments of stained organic material not completely adhered to the MSNs surface were also observed. As previously reported, this could be attributed to the possibility of an excess of cell membrane which, above a certain amount, tend to self-aggregate decreasing the efficient interaction with the NPs surface [59].

The presence of the cell membrane coating was further confirmed by thermogravimetric analyses. The results are shown in Table 1 as relative percentage increase of organic matter compared to the unloaded, uncoated amino-functionalized MSNs. The results highlight both the capacity of MSNs as nanocarrier, displaying the amount of loaded calcein and the success of coating with cell membranes. The percentage increase of organic matter due only to cell membrane coating can be extrapolated from these values, when comparing to MSNs@CAL samples. The accuracy of the extrapolated values was confirmed by the analysis of the sample without calcein (data not shown). Interestingly, for both types of amino functionalization, the highest value of organic matter were detected for MSNs coated with 1 and 4 million cells and it decreased for higher membrane amounts. In general MSN-NH-$NH_2$@CAL–MC3T3-E1 samples presented higher percentages increase with respect to the MSNs-$NH_2$@CAL–MC3T3-E1 counterparts. However, it should be considered that the technique quantifies all the organic content of the sample and the percentage increase thus includes the contribution of both cell membrane coating and loaded calcein. Considering the uncoated loaded nanoparticles, DAMO functionalized MSNs (MSNs-NH-$NH_2$@CAL) showed a far higher percentage increase than those functionalized with APTES (MSNs-$NH_2$@CAL). In view of these values, MSNs-$NH_2$@CAL–MC3T3-E1 samples actually presented a larger percentage increase ascribable to cell membrane coating than those functionalized with DAMO.

DLS measurements evidenced no significant changes in the hydrodynamic size distribution of coated MSNs, all fluctuating between 215 nm and 296 nm (Table 1). These results show that the developed procedure allows the coating of individual MSNs without leading to aggregation and provides monodisperse MSNs in the nanometric range suitable for biological applications. More interestingly, the surface charge of membrane-coated MSNs decreased compared to the uncoated ones, suggesting the presence of negatively charged membranes and, therefore, the success of the coating process. In particular, APTES functionalized MSNs showed increasingly negative Z-potential values when combined with MC3T3-E1 cell membrane from 1 to 14 million, whereas DAMO functionalized MSNs showed decreasingly positive values (Table 1). Reasonably, these trends could be attributed to a higher quantity of cell membrane attached to the MSNs surface, forming an increasingly dense coating layer. Both types of MSNs coated with membranes from 21 million of cells showed lower Z-potential values than naked MSNs, but the reduction was lower compared to the samples coated with less membrane. Also, TGA results showed a decrease in the organic matter for samples coated with high membrane ratios and together these results indicate a threshold in the suitable amount of coating material. As already observed by TEM analyses, larger amounts of cell membranes could result in an excess of material, which causes the self-assembly of membrane fragments and could hinder their interaction with the MSNs surface. Moreover, it is interesting to note the difference between the APTES functionalized MSNs, which shift their surface charge to negative when coated with all the tested ratios of MC3T3-E1 cell membranes, and DAMO functionalized MSNs, which decrease their surface charge after the coating but remain positive. This behavior could be easily attributed to the initial surface charge of MSNs, since MSNs functionalized with DAMO have a higher Z-Potential value than those functionalized with APTES.

Finally, FT-IR spectra of all coated MSNs (Fig. S1C,D) were characterized by an increase of the vibration bands between 3200 and 3650 $cm^{-1}$, ascribable to the stretching vibration bands from –OH groups present in phospholipids and other surface molecules of cell membranes.

Overall, all physicochemical characterization techniques indicate a strong interaction between preosteoblastic cell membranes and amino-functionalized MSNs, suggesting the validity of the developed approach for the formation of an effective coating. The release capability, investigated in the next section, was identified as key parameter for establishing the optimal formulation of membrane coated MSNs, as it can indirectly provide information about the homogeneity and efficiency of the coating and allow to optimize the formulation in the perspective of its application as a drug delivery system.

### 3.3. Effect of cell membrane coating on cargo release

Cargo release assay using calcein as drug model was performed monitoring the overtime release from both MSNs uncoated and coated with different ratios of MC3T3-E1 cell membranes. Calcein was chosen as cargo model molecule because of its inability to cross lipid bilayers. This property was exploited to validate the formation, stability and disruption of the MSNs coating. In principle, the cell membrane layer should efficiently shield the MSN surface

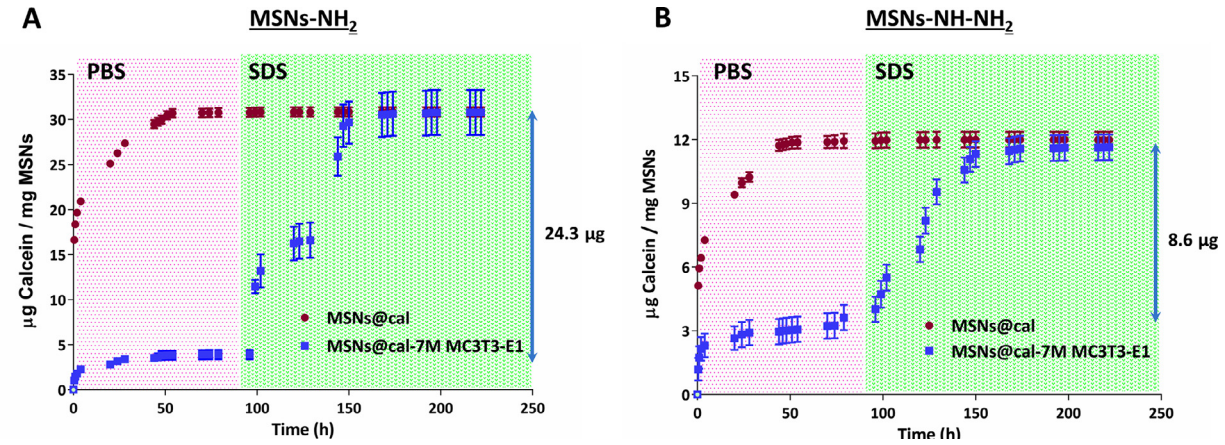


**Fig. 2.** Overtime cumulative calcein release expressed as µg calcein/mg MSNs of uncoated and cell membrane-coated MSNs. **(A)** APTES functionalized MSNs (MSNs@cal) and APTES functionalized MSNs coated with MC3T3-E1 cell membranes from 7 million of cells (MSNs@cal-7M MC3T3-E1). **(B)** DAMO functionalized MSNs (MSNs@cal) and DAMO functionalized MSNs coated with MC3T3-E1 cell membranes from 7 million of cells (MSNs@cal-7M MC3T3-E1). All the samples were maintained in PBS (pH = 7.4) for the first 72 h and in SDS solution (0.5% in PBS) thereafter. Results are represented as mean ± SD of three experiments.

and block the pore entrances, providing a barrier against calcein diffusion and premature release.

As represented in Fig. 2, both uncoated APTES and DAMO functionalized MSNs presented a continuous release up to 48 h with the typical diffusion release profile from the mesoporous channels of MCM41-like NPs (red dots in Fig. 2A and B, respectively) [54]. Interestingly, the amount of calcein released form MSNs-$NH_2$ was higher than that released from MSNs-NH-$NH_2$. This may be attributed to the higher positive charge of DAMO functionalized MSNs which can interact more strongly with the negative calcein molecules, partially hindering their release.

In contrast, all membrane coated MSNs presented a small initial release, probably due to calcein molecules adsorbed on the membrane layer or leaked from areas of incomplete coating. However, during the first few hours all coated-MSNs reached a plateau with no detectable calcein release, which remained constant until the end of monitoring without the addition of SDS (see Fig. S3A–J in the Supporting Information). This profile is consistent with the inability of calcein to diffuse through lipid bilayers and clearly demonstrates the success of the coating procedure, in which cell membranes provide an effective barrier against premature cargo release.

Conversely, coated MSNs immersed in PBS solution with SDS, an anionic surfactant capable of disrupting plasma membranes and increasing their permeability, displayed a rapid release profile with a burst in the first few hours after SDS addition and reaching a second plateau (blue square in Fig. 2A,B). The coated membrane acted as a physical barrier to impede the premature release of the cargo molecules, rather than to potentially modify the release kinetics of the developed system.

The release assay further confirms the success of the coating procedure and allows an indirect quantification of the coating efficiency. The amount of calcein released after the SDS addition was directly correlated with the coating efficiency. Indeed, larger and more homogenous amount of cell membranes shielding the MSNs would ensure the retaining of higher amounts of cargo in the pores, leading to superior extent of release after the destruction of the coating by SDS. The results of the release assay from APTES and DAMO functionalized MSNs coated with different ratios of MC3T3-E1 cell membranes are shown in Fig. S3A–J. For all membrane amounts, coated MSNs-$NH_2$ were found to release higher quantities of calcein with respect to MSNs-NH-$NH_2$. This is particularly interesting considering that thermogravimetric analysis showed lower loading amounts for MSNs-$NH_2$@CAL and suggests a preferential interaction of cell membranes with APTES functionalized MSNs. The results could be possibly explained by the higher positive surface charge of DAMO functionalized MSNs which, contrary to expectations, did not result in a better coating. In this regard, an interesting study from the literature reported that high Z-potential values can actually generate too strong electrostatic interactions hindering the proper arrangement of membranes bilayer for complete NPs coverage [60].

Considering the different membranes ratios, both types of MSNs showed the same trend with higher amount of calcein released from samples coated with 7 million of MC3T3-E1 source cells, closely followed by 14, 21, 4 and 1 million. As shown in Figs. 2A and S3E, MSNs-$NH_2$@CAL–7M MC3T3-E1 was the sample with best performances, able to release up to 24.3 µg calcein/mg MSNs, and it was therefore selected as the optimal formulation for the following *in vitro* assays.

### *3.4. Biocompatibility of different cell lines treated with membrane-coated and non-coated MSNs*

The biocompatibility of these nanosystems can be assessed by studying cell viability when cells are exposed to these nanoparticles as this is related to the integrity of the cytoplasmic membrane. Therefore, cell viability was studied in different cell lines such as MC3T3-E1 from which the cell membrane was extracted for coating and two other different cell lines such as HeLa and HGUE-GB-39. These cells were seeded in 96-well plates and exposed to different concentrations (1, 2.5, 5, 10, 25, 50 and 75 µg/mL) of uncoated and membrane-coated MSNs for 3 h. Fig. 3 shows that uncoated MSNs were not cytotoxic up to 50 ug/mL in any cell line. However, when the cells were exposed to a concentration of 75 ug/mL, a decrease in cell viability of 25% was observed. On the other hand, membrane-coated MSNs were not cytotoxic in HeLa and HGUE-GB-39 cells as there was only a slight decrease of viability in all the concentrations. Furthermore, these coated MSNs showed that they were not toxic in MC3T3-E1 cells, since at a dose of 25 ug/mL there was 89% proliferation. In contrast, a decrease in viability of these cells was observed from this dose onwards, possibly because there was an increased interaction of the coated MSNs with their cell line of origin and also because at higher concentrations of these MSNs, small aggregates were formed that may be affecting viability. In addition, previous articles have shown that these uncoated MSNs were not toxic at high concentrations [40]. This difference in cytotoxicity between

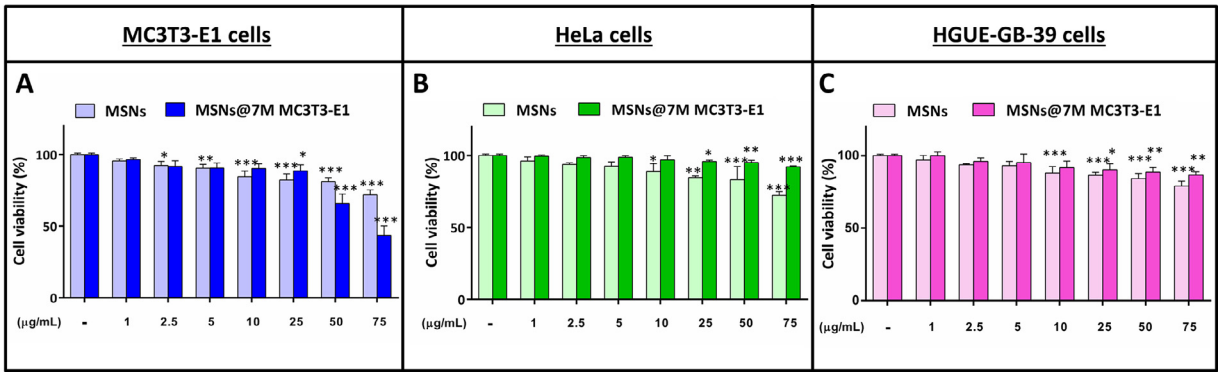


**Fig. 3.** Cell viability in different cell lines with coated and uncoated MSNs. **(A)** MC3T3-E1, **(B)** HeLa and **(C)** HGUE-GB-39 cells were incubated with MSNs or MSNs@7M MC3T3-E1 at different concentrations (1, 2.5, 5, 10, 25, 50 and 75 μg/mL) for 3 h. After this time, viability was assessed in all samples. Cells cultured without nanoparticles were used as control (−). Data are means ± SD of three independent experiments. Statistical significance: $^{*}P < 0.05$, compared with the control; $^{**}P < 0.01$, compared with the control; $^{***}P < 0.001$, compared with the control.

cell lines when treated with membrane-coated MSNs from MC3T3-E1 is because there is a higher internalization of these MSNs in the MC3T3-E1 cell line than in the other two cell lines. Additionally, due to the phenotypic characteristics presented by the MC3T3-E1 cell line (pre-osteoblasts), these cells are not differentiated. However, the other two cell lines (HeLa and HGUE-GB-39) are tumor cells and are differentiated. This means that the MC3T3-E1 cell line is more sensitive in response to the different nanosystems [61].

### *3.5. Effects of membrane-coated MSNs on oxidative stress and cell cycle in MC3T3-E1 pre-osteoblastic cells*

Based on the biocompatibility results, the response of pre-osteoblastic cells (MC3T3-E1) exposed to a maximum concentration of 25 μg/mL of membrane-coated MSNs was investigated though intracellular production of reactive oxygen species (ROS). Additionally, the effect on cell cycle was evaluated by flow cytometry after exposure to these nanocarriers. First, a study of ROS production was performed because nanoparticles have a high tendency to produce large amounts of reactive oxygen species. As a consequence of their strong oxidation potential, excess ROS induced by MSNs can cause damage to biomolecules and organelle structures, leading to lipid peroxidation, oxidative carbonylation of proteins, DNA/RNA breakage and even destruction of membrane structure, which in turn leads to necrosis, apoptosis or mutagenesis [62]. Figs. 4A and S4 show the percentage of the pre-osteoblast cell population with intracellular ROS content. After exposure to coated and uncoated MSNs for 3h, no significant differences were observed with respect to untreated cells. Thus, it was confirmed that our nanomaterials did not affect the percentage of ROS population after exposure. Fig. 4B shows the intracellular ROS content (intensity, arbitrary units (A.U.)) of MC3T3-E1 cells after treatment with the different samples. In this case, a significant increase in ROS intensity was observed in cells treated with the different MSNs, the highest being the 25 ug/mL concentration of MSNs@7M MC3T3-E1. However, although there were elevated ROS values, no decrease in cell viability was obtained for these concentrations as seen above (Fig. 3), so the coated and uncoated MSNs appear to be non-cytotoxic. These ROS values do not need to be associated with a cytotoxic response of MSNs, as a large number of cell lines retain a basal expression of ROS as a result of the mitochondrial electron transport chain, necessary to catabolize amino acids, fatty acids and carbohydrates [63]. Additionally, these ROS values could be elevated during the proliferation process due to the bioenergetic requirement needed for cell cycle progression [64].

Secondly, a cell cycle study was performed to verify that membrane-coated and uncoated MSNs were not cytotoxic and did not affect the proper cellular functioning of these cells. For this purpose, the same concentrations were used as for ROS production evaluation. Fig. 4**C** shows that direct contact between MC3T3-E1 cells and coated or uncoated MSNs did not significantly modify their cell cycle so that the correct functioning of these cells is maintained. In conclusion, the treatment of cells with these concentrations of uncoated and coated MSNs does not generate a cytotoxic response in the MC3T3-E1 cell line.

### *3.6. Enhanced cellular uptake of membrane-coated MSNs by MC3T3-E1 cells*

The cellular uptake by different cell lines of uncoated and cell membrane-coated MSNs was quantitatively evaluated by means of flow cytometry and qualitatively analyzed by confocal microscopy. Fig. 5**A–C** depicts the total percentage of the cell population that internalized the MSNs, measured as FITC fluorescence. The naked MSNs were internalized by all the cell lines in an equivalent manner, with an observed increase in internalization proportional to the increase in the MSNs concentration used. As per the membrane-coated MSNs, they were internalized by a significantly higher number of cells only in the case of the MC3T3-E1 cells, compared to the naked MSNs. The maximum values of internalization were achieved when using concentrations equal to or higher than 10 ug/mL. Interestingly, the membrane-coated MSNs showed higher values of internalization in the MC3T3-E1 cell line than on the HeLa or HGUE-GB-39 cells. In these two cell lines, the presence of the cell membrane on the surface of the MSNs reduced the cellular uptake by approximately 50%, compared to the MC3T3-E1 cells. Surprisingly, the same reduction in internalization was observed when compared to the naked MSNs. These results indicate that the cell membrane-coating not only enhances the internalization of the MSNs by a specific cellular population (the source cells) but also disadvantages the uptake by other cell types. The cell membrane-coating masks the positive charge of the nanoparticles, which is known to favor cellular internalization. Consequently, this biomimetic technology could potentially be used for increasing targeting efficacy of NPs while diminishing undesired unspecific interactions, which would increase the safety and efficiency of the nanosystem.

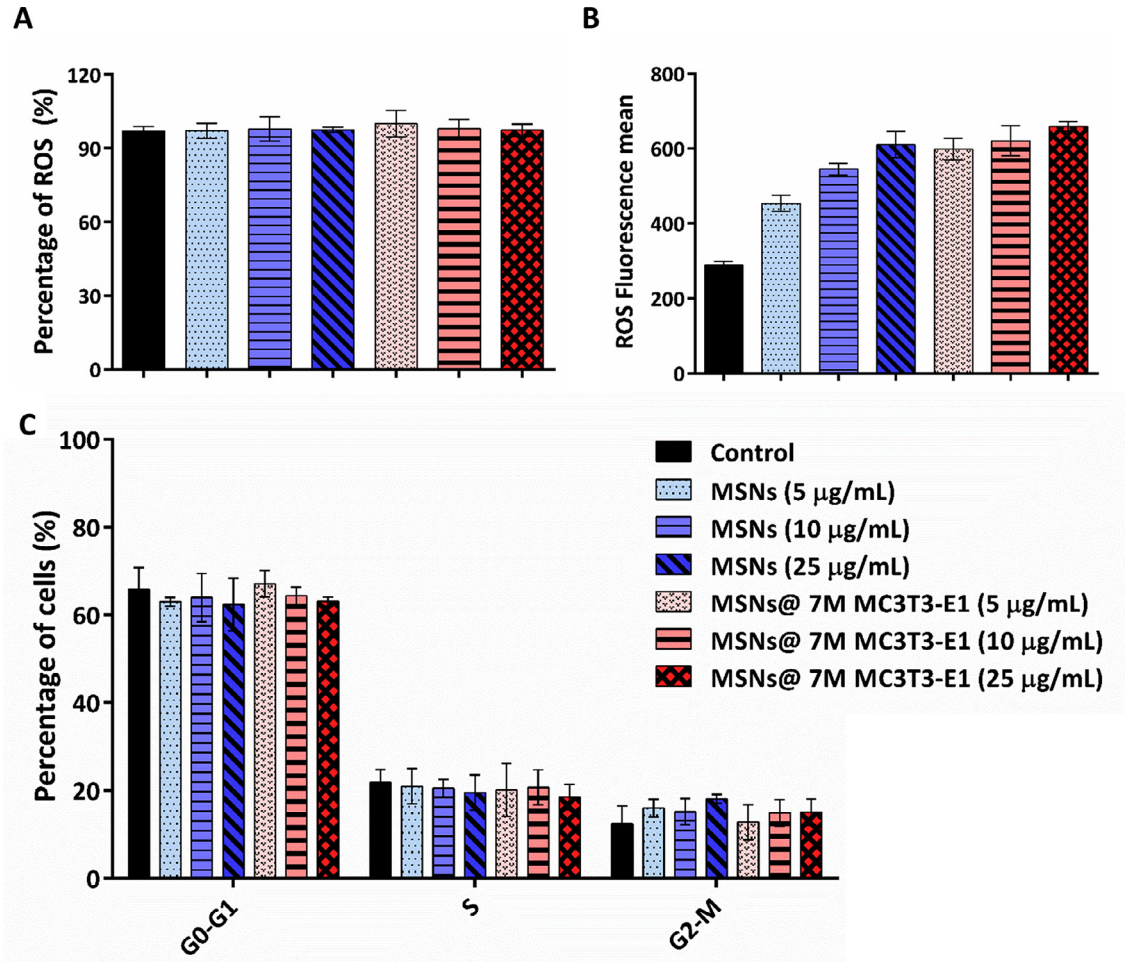


**Fig. 4.** Effects of MSNs or MSNs@7M MC3T3-E1 on ROS and cell cycle. MC3T3-E1 cells were incubated with coated and uncoated MSNs at different concentrations (5, 10, 25 μg/mL) for 3 h and then analyzed. Measurement of ROS production expressed as **(A)** percentages of ROS positive cells and **(B)** mean fluorescence intensity obtained by flow cytometry. **(C)** Cell cycle analysis by flow cytometry. The phases of the cell cycle are composed of G0, G1, S, G2 and M. Quiescent cells are stationary in G0 phase. If the cell cycle is activated, the cell enters the G1 phase (cell growth) and prepares for DNA synthesis, which occurs in the S phase. In G2 phase the chromosomes have already been replicated, and the cell prepares for mitosis (M). Data are means ± SD of three independent experiments. Statistical significance: $^{***}P < 0.001$, compared with the control.

The total amount of MSNs internalized by the cells was quantified as the mean fluorescence intensity of the cells (Fig. 5D–F). In the case of the MC3T3-E1 cells, the total number of internalized MSNs increased very significantly when the MSNs were coated with the cell membranes, complementing the previous results, and indicating an enhanced cellular uptake effect. Additionally, an increase was observed with the concentration used up to 25 ug/mL, after which it diminished in agreement with the observed reduced viability (see Fig. 3A). In the case of the HeLa and HGUE-GB-39 cultures, no difference was observed between the coated and uncoated MSNs, indicating no effect of the cell membrane-coating on the total uptake of MSNs when exposed to different cell lines other than the source cell one.

Confocal imaging qualitatively confirmed the preferential internalization of the nanoparticles into the preosteoblastic cells (Fig. 5G). Both coated and uncoated MSNs were observed within the cytoplasm of the cells. The uncoated MSNs were observed qualitatively within similar amounts in all cell lines while the cell membrane-coated MSNs were observed in a considerably higher amount in the MC3T3-E1 cells. These observations indicated once more the preference the nanosystems display for the membrane-coating source cell type, in agreement with the above showed results and the literature.

### *3.7. Preferential migration of MC3T3-E1 membrane-coated MSNs towards MC3T3-E1 cells*

The migration tendencies of the coated and uncoated MSNs towards the different cell lines were assessed with an *in vitro* migration model (Fig. 6A). After 24 h of exposure, the percentage of MSNs that had crossed the transwell membrane towards the targeted cells was quantified via fluorescence microscopy (Fig. 6B). A significant tendency of the coated MSNs to migrate towards the MC3T3-E1 cells was observed, as indicated by the lowest percentage remaining above the transwell membrane (Fig. 6C). However, in line with the internalization results, the opposite was observed when the MSNs were exposed to HeLa and HGUE-GB-39 cells. Interestingly, the presence of the MC3T3-E1 cell membrane-coating seemed to hinder the migration of the MSNs towards other cell lines compared to the naked nanoparticles, to the point where no significant migration whatsoever was observed. A slight migration was observed with the naked MSNs compared to the control in all cases. The negligible percentage of MSNs inside the transwell membranes and on the media of the wells (Fig. 6D,E) indicated that the MSNs that had migrated towards the cells had been also internalized by the same, in all cases.

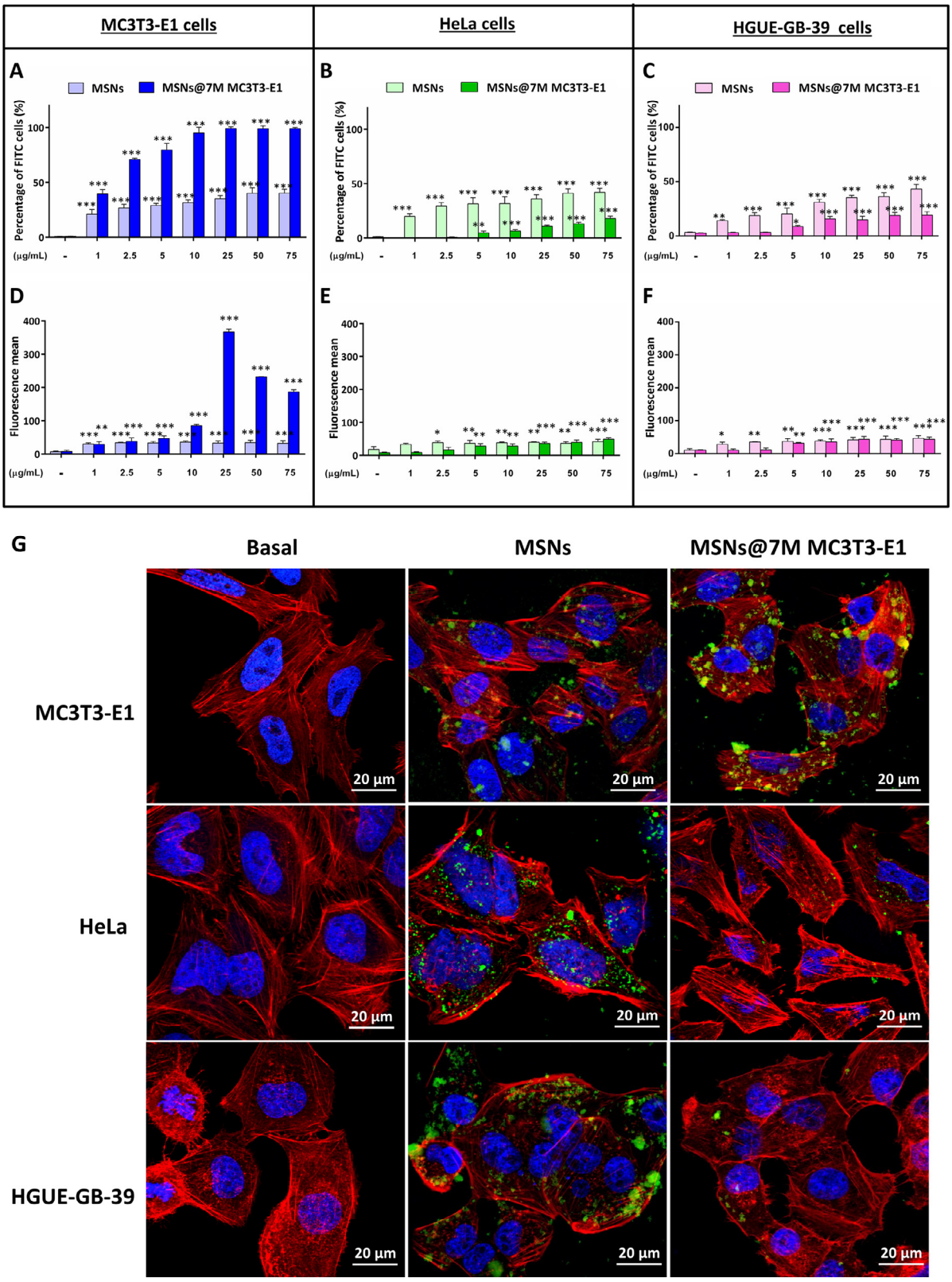


**Fig. 5.** Cellular uptake of coated and uncoated MSNs in different cell types. Flow cytometry results expressed in percentages of positive events in **(A)** MC3T3-E1, **(B)** HeLa and **(C)** HGUE-GB-39 cells after 3 h of treatment with the different concentrations of FITC-labelled MSNs or MSNs@7M MC3T3-E1 (1, 2.5, 5, 10, 25, 50 and 75 μg/mL). Quantitative analysis of the mean fluorescence intensity of FITC in the different lines **(D, E** and **F)** was obtained by flow cytometry. Cells cultured without nanoparticles were used as control (−). Data are means ± SD of three independent experiments. Statistical significance: $^{*}P < 0.05$; $^{**}P < 0.01$; $^{***}P < 0.001$, all compared with the control. **(G)** Representative images of internalization in different cell lines by confocal microscopy. Cells were treated with MSNs or MSNs@7M MC3T3-E1 (75 μg/mL) for 3h and cells cultured without nanoparticles were used as control. The fluorescence signals of DAPI (blue), FITC (green), and phalloidin (red) were examined under a confocal laser scanning microscope. The images shown are the merge of the 3 channels. Legend, from left to right: The first column shows the different untreated cell lines. The second column shows cells treated with MSNs and the third column shows cells treated with MSNs@7M MC3T3-E1. Bar 20 μm.

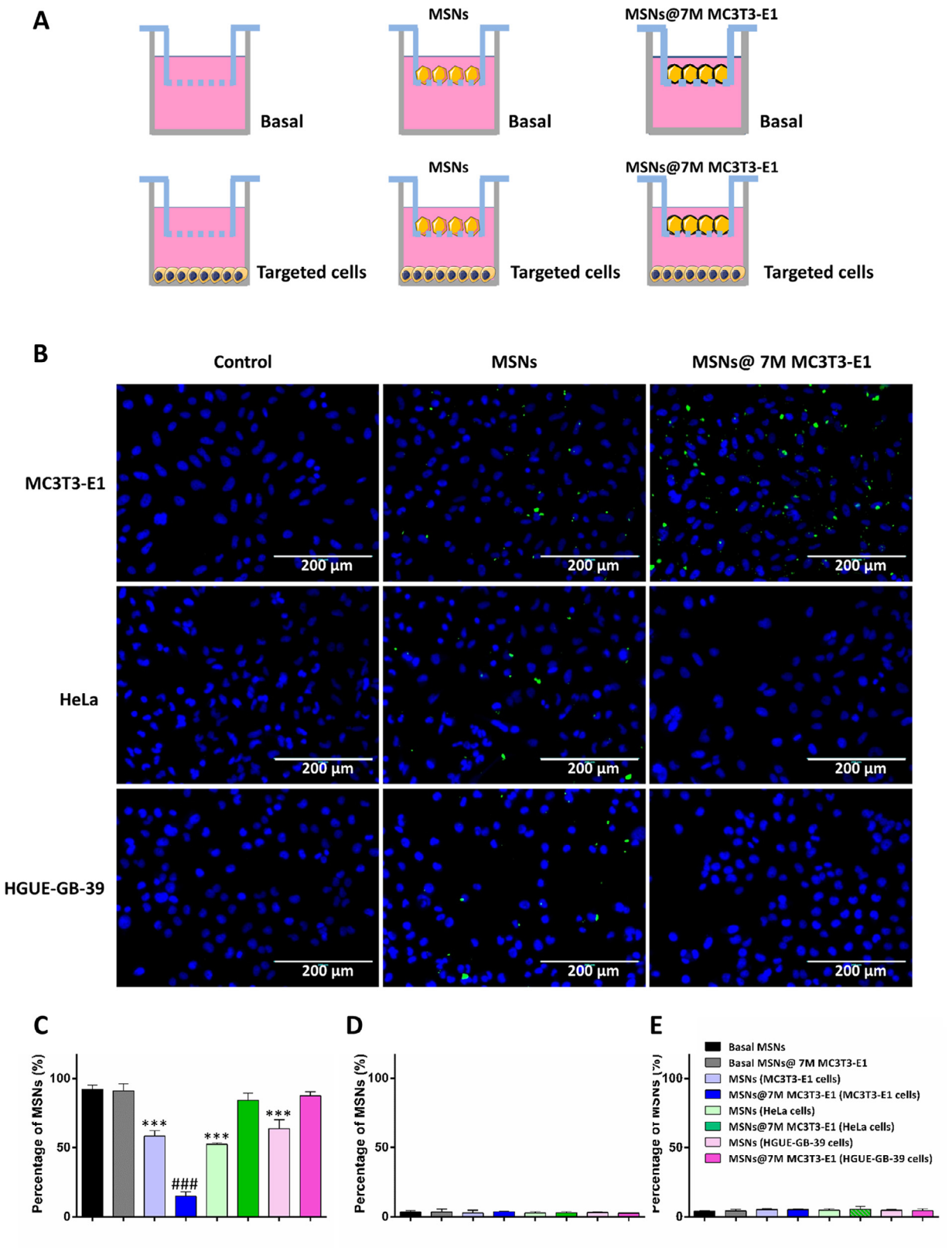


**Fig. 6.** **(A)** Transwell cell migration assay. **(B)** Migration of MSNs or MSNs@7M MC3T3-E1 to the different cell lines with nuclei staining (DAPI) after 24 h exposure. Scale bars, 200 µm. Percentage of MSNs **(C)** above, **(D)** inside or **(E)** below the transwell membrane quantified using a Biotek Synergy 4 microplate reader (excitation/emission: 490/520 nm). Data are means ± SD of three independent experiments. Statistical significance: $^{***}P < 0.001$; $^{###}P < 0.001$, all compared to their respective control

Overall, the above results indicate a direct effect or interaction of the cell membrane-coating with the source cell type. This opens the possibility of employing this technology to directly target and interact with specific cell types while avoiding unspecific interactions.

## 4. Conclusion

We have developed and characterized a versatile nanocarrier platform able to combine the benefits from mesoporous silica nanoparticles, such as robustness and high loading capacity, together with the outstanding biological properties from cell membranes, such as biocompatibility and migration capacity. The synthetic method for the presented nanoplatform was optimized and it could easily be applicable for coating MSNs with different cell membranes from a variety of sources. The pores of the nanocarriers could be loaded with many different types of therapeutic agents without any type of premature release, which would only take place after the controlled disruption of the coating membrane.

The designed nanoparticles showed internalization selectivity towards the very same cells than those employed as source for the coating membrane of the nanocarriers, which could be of interest for future selective treatments. More interestingly, the designed nanocarriers showed selective migration properties towards those cells employed as source for coating the nanoconstructs, which could be of extreme importance for future selective treatments, such as potential cancer treatment. As a potential application, nanosystems coated with cell membranes obtained from a patient's biopsy could be employed to target them towards a specific tissue, tumor, or even metastatic niche, as cell membranes are known to be involved in cancer metastasis. Thus, the cell membrane-coating nanotechnology could be the answer to personalized, patient-focused nanomedicine.

## Declaration of Competing Interest

The authors have no competing interest to declare.

## Acknowledgments

This research was funded by European Research Council (Advanced Grant VERDI; ERC-2015-AdG) grant number [694160] and the Spanish "Ministerio de Ciencia e Innovación" through the project PID2019-106436RB-I00 (Agencia Estatal de Investigación, AEI/10.13039/501100011033).

## Supplementary materials

Supplementary material associated with this article can be found, in the online version, at doi:10.1016/j.actbio.2022.11.059.

## References

[1] E.K. Lim, T. Kim, S. Paik, S. Haam, Y.M. Huh, K. Lee, Nanomaterials for theranostics: recent advances and future challenges, Chem. Rev. 115 (2015) 327–394, doi:10.1021/cr300213b.
[2] M.J. Mitchell, M.M. Billingsley, R.M. Haley, M.E. Wechsler, N.A. Peppas, R. Langer, Engineering precision nanoparticles for drug delivery, Nat. Rev. Drug Discov. 20 (2021) 101–124, doi:10.1038/s41573-020-0090-8.
[3] E. Blanco, H. Shen, M. Ferrari, Principles of nanoparticle design for overcoming biological barriers to drug delivery, Nat. Biotechnol. 33 (2015) 941–951, doi:10.1038/nbt.3330.
[4] B. Dumontel, F. Susa, T. Limongi, V. Vighetto, D. Debellis, M. Canta, V. Cauda, Nanotechnological engineering of extracellular vesicles for the development of actively targeted hybrid nanodevices, Cell Biosci. 12 (2022) 61, doi:10.1186/s13578-022-00784-9.
[5] F. Gao, L. Xu, B. Yang, F. Fan, L. Yang, Kill the real with the fake: eliminate intracellular staphylococcus aureus using nanoparticle coated with its extracellular vesicle membrane as active-targeting drug carrier, ACS Infect. Dis. 5 (2019) 218–227, doi:10.1021/acsinfecdis.8b00212.
[6] C. Jiménez-Jiménez, M. Manzano, M. Vallet-Regí, Nanoparticles coated with cell membranes for biomedical applications, Biology 9 (2020) 406 (Basel), doi:10.3390/biology9110406.
[7] L. Rao, L.L. Bu, J.H. Xu, B. Cai, G.T. Yu, X. Yu, Z. He, Q. Huang, A. Li, S.S. Guo, W.F. Zhang, W. Liu, Z.J. Sun, H. Wang, T.H. Wang, X.Z. Zhao, Red blood cell membrane as a biomimetic nanocoating for prolonged circulation time and reduced accelerated blood clearance, Small 11 (2015) 6225–6236, doi:10.1002/smll.201502388.
[8] R.H. Fang, C.M.J. Hu, B.T. Luk, W. Gao, J.A. Copp, Y. Tai, D.E. O'Connor, L. Zhang, Cancer cell membrane-coated nanoparticles for anticancer vaccination and drug delivery, Nano Lett. 14 (2014) 2181–2188, doi:10.1021/nl500618u.
[9] P.V Escribá, J.M. González-Ros, F.M. Goñi, P.K.J. Kinnunen, L. Vigh, L. Sánchez-Magraner, A.M. Fernández, X. Busquets, I. Horváth, G. Barceló-Coblijn, Membranes: a meeting point for lipids, proteins and therapies, J. Cell. Mol. Med. 12 (2008) 829–875, doi:10.1111/j.1582-4934.2008.00281.x.
[10] M.V Farrell, S. Webster, K. Gaus, J. Goyette, T cell membrane heterogeneity aids antigen recognition and T cell activation, Front. Cell Dev. Biol. 8 (2020) 609, doi:10.3389/fcell.2020.00609.
[11] J. Liu, A. Stace-Naughton, X. Jiang, C.J. Brinker, Porous nanoparticle supported lipid bilayers (protocells) as delivery vehicles, J. Am. Chem. Soc. 131 (2009) 1354–1355, doi:10.1021/ja808018y.
[12] A. Luchini, G. Vitiello, Understanding the nano-bio interfaces: lipid-coatings for inorganic nanoparticles as promising strategy for biomedical applications, Front. Chem. 7 (2019) 343, doi:10.3389/fchem.2019.00343.
[13] X.L. Hu, N. Kwon, K.C. Yan, A.C. Sedgwick, G.R. Chen, X.P. He, T.D. James, J. Yoon, Bio-conjugated advanced materials for targeted disease theranostics, Adv. Funct. Mater. 30 (2020) 1907906, doi:10.1002/adfm.201907906.
[14] C.M.J. Hu, Z. Li, A. Santosh, C. Connie, R.H. Fang, Z. Liangfang, Erythrocyte membrane-camouflaged polymeric nanoparticles as a biomimetic delivery platform, Proc. Natl. Acad. Sci. 108 (2011) 10980–10985, doi:10.1073/pnas.1106634108.
[15] V.R. Muzykantov, Drug delivery by red blood cells: vascular carriers designed by mother nature, Expert Opin. Drug Deliv. 7 (2010) 403–427, doi:10.1517/17425241003610633.
[16] J.G. Piao, L. Wang, F. Gao, Y.Z. You, Y. Xiong, L. Yang, Erythrocyte membrane is an alternative coating to polyethylene glycol for prolonging the circulation lifetime of gold nanocages for photothermal therapy, ACS Nano 8 (2014) 10414–10425, doi:10.1021/nn503779d.
[17] Y. Wang, K. Zhang, X. Qin, T. Li, J. Qiu, T. Yin, J. Huang, S. McGinty, G. Pontrelli, J. Ren, Q. Wang, W. Wu, G. Wang, Biomimetic nanotherapies: red blood cell based core–shell structured nanocomplexes for atherosclerosis management, Adv. Sci. 6 (2019) 1900172, doi:10.1002/advs.201900172.
[18] A. Parodi, N. Quattrocchi, A.L. van de Ven, C. Chiappini, M. Evangelopoulos, J.O. Martinez, B.S. Brown, S.Z. Khaled, I.K. Yazdi, M.V. Enzo, L. Isenhart, M. Ferrari, E. Tasciotti, Synthetic nanoparticles functionalized with biomimetic leukocyte membranes possess cell-like functions, Nat. Nanotechnol. 8 (2013) 61–68, doi:10.1038/nnano.2012.212.
[19] J. Lopes, D. Lopes, M. Pereira-Silva, D. Peixoto, F. Veiga, M.R. Hamblin, J. Conde, C. Corbo, E.N. Zare, M. Ashrafizadeh, F.R. Tay, C. Chen, R.F. Donnelly, X. Wang, P. Makvandi, A.C. Paiva-Santos, Macrophage cell membrane-cloaked nanoplatforms for biomedical applications, Small Methods 6 (2022) 2200289, doi:10.1002/smtd.202200289.
[20] C.M.J. Hu, R.H. Fang, K.C. Wang, B.T. Luk, S. Thamphiwatana, D. Dehaini, P. Nguyen, P. Angsantikul, C.H. Wen, A.V Kroll, C. Carpenter, M. Ramesh, V. Qu, S.H. Patel, J. Zhu, W. Shi, F.M. Hofman, T.C. Chen, W. Gao, K. Zhang, S. Chien, L. Zhang, Nanoparticle biointerfacing by platelet membrane cloaking, Nature 526 (2015) 118–121, doi:10.1038/nature15373.
[21] Q. Hu, W. Sun, C. Qian, C. Wang, H.N. Bomba, Z. Gu, Anticancer platelet-mimicking nanovehicles, Adv. Mater. 27 (2015) 7043–7050, doi:10.1002/adma.201503323.
[22] L. Xu, F. Gao, F. Fan, L. Yang, Platelet membrane coating coupled with solar irradiation endows a photodynamic nanosystem with both improved antitumor efficacy and undetectable skin damage, Biomaterials 159 (2018) 59–67, doi:10.1016/j.biomaterials.2017.12.028.
[23] C. Gao, Z. Lin, B. Jurado-Sánchez, X. Lin, Z. Wu, Q. He, Stem cell membrane-coated nanogels for highly efficient *in vivo* tumor targeted drug delivery, Small 12 (2016) 4056–4062, doi:10.1002/smll.201600624.
[24] Z. Gao, L. Zhang, J. Hu, Y. Sun, Mesenchymal stem cells: a potential targeted-delivery vehicle for anti-cancer drug, loaded nanoparticles, Nanomedicine 9 (2013) 174–184, doi:10.1016/j.nano.2012.06.003.
[25] I. Ferreira-Faria, S. Yousefiasl, A. Macário-Soares, M. Pereira-Silva, D. Peixoto, H. Zafar, F. Raza, H. Faneca, F. Veiga, M.R. Hamblin, F.R. Tay, J. Gao, E. Sharifi, P. Makvandi, A.C. Paiva-Santos, Stem cell membrane-coated abiotic nanomaterials for biomedical applications, J. Control. Release 351 (2022) 174–197, doi:10.1016/j.jconrel.2022.09.012.
[26] J. Zhang, Y. Miao, W. Ni, H. Xiao, J. Zhang, Cancer cell membrane coated silica nanoparticles loaded with ICG for tumour specific photothermal therapy of osteosarcoma, Artif. Cells Nanomed. Biotechnol. 47 (2019) 2298–2305, doi:10.1080/21691401.2019.1622554.
[27] W. Gao, L. Zhang, Coating nanoparticles with cell membranes for targeted drug delivery, J. Drug Target. 23 (2015) 619–626, doi:10.3109/1061186X.2015.1052074.
[28] M. Ashrafizadeh, M. Delfi, A. Zarrabi, A. Bigham, E. Sharifi, N. Rabiee, A.C. Paiva-Santos, A.P. Kumar, S.C. Tan, K. Hushmandi, J. Ren, E.N. Zare, P. Makvandi, Stimuli-responsive liposomal nanoformulations in cancer therapy: pre-

clinical & clinical approaches, J. Control. Release Off. J. Control. Release Soc. 351 (2022) 50–80, doi:10.1016/j.jconrel.2022.08.001.
[29] H. Sun, J. Su, Q. Meng, Q. Yin, L. Chen, W. Gu, P. Zhang, Z. Zhang, H. Yu, S. Wang, Y. Li, Cancer-cell-biomimetic nanoparticles for targeted therapy of homotypic tumors, Adv. Mater. 28 (2016) 9581–9588, doi:10.1002/adma.201602173.
[30] D. Wang, S. Wang, Z. Zhou, D. Bai, Q. Zhang, X. Ai, W. Gao, L. Zhang, White blood cell membrane-coated nanoparticles: recent development and medical applications, Adv. Healthc. Mater. 11 (2022) 2101349, doi:10.1002/adhm.202101349.
[31] M.G. Jakaria, P. Sorkhdini, D. Yang, Y. Zhou, S.A. Meenach, Lung cell membrane-coated nanoparticles capable of enhanced internalization and translocation in pulmonary epithelial cells, Int. J. Pharm. 613 (2022) 121418, doi:10.1016/j.ijpharm.2021.121418.
[32] L. Zhu, Y. Zhong, S. Wu, M. Yan, Y. Cao, N. Mou, G. Wang, D. Sun, W. Wu, Cell membrane camouflaged biomimetic nanoparticles: focusing on tumor theranostics, Mater. Today. Bio. 14 (2022) 100228, doi:10.1016/j.mtbio.2022.100228.
[33] M. Pereira-Silva, A.C. Santos, J. Conde, C. Hoskins, A. Concheiro, C. Alvarez-Lorenzo, F. Veiga, Biomimetic cancer cell membrane-coated nanosystems as next-generation cancer therapies, Expert Opin. Drug Deliv. 17 (2020) 1515–1518, doi:10.1080/17425247.2020.1813109.
[34] F. Farjadian, M. Moghoofei, S. Mirkiani, A. Ghasemi, N. Rabiee, S. Hadifar, A. Beyzavi, M. Karimi, M.R. Hamblin, Bacterial components as naturally inspired nano-carriers for drug/gene delivery and immunization: Set the bugs to work? Biotechnol. Adv. 36 (2018) 968–985, doi:10.1016/j.biotechadv.2018.02.016.
[35] R. Zhang, S. Wu, Q. Ding, Q. Fan, Y. Dai, S. Guo, Y. Ye, C. Li, M. Zhou, Recent advances in cell membrane-camouflaged nanoparticles for inflammation therapy, Drug Deliv. 28 (2021) 1109–1119, doi:10.1080/10717544.2021.1934188.
[36] Y. Zhang, H. Yang, D. Wei, X. Zhang, J. Wang, X. Wu, J. Chang, Mitochondria-targeted nanoparticles in treatment of neurodegenerative diseases, Exploration 1 (2021) 20210115, doi:10.1002/EXP.20210115.
[37] European Commission, Directorate-General for Research and Innovation, Population ageing in Europe: facts, implications and policies: outcomes of EU–funded research, Publications Office of the European Union, 2014 https://data.europa.eu/doi/10.2777/60452.
[38] M. Gisbert-Garzarán, M. Manzano, M. Vallet-Regí, Mesoporous silica nanoparticles for the treatment of complex bone diseases: bone cancer, bone infection and osteoporosis, Pharmaceutics 12 (2020), doi:10.3390/pharmaceutics12010083.
[39] P. Mora-Raimundo, M. Manzano, M. Vallet-Regí, Nanoparticles for the treatment of osteoporosis, AIMS Bioeng. 4 (2017) 259–274, doi:10.3934/bioeng.2017.2.259.
[40] E. Álvarez, M. Estévez, C. Jiménez-Jiménez, M. Colilla, I. Izquierdo-Barba, B. González, M. Vallet-Regí, A versatile multicomponent mesoporous silica nanosystem with dual antimicrobial and osteogenic effects, Acta Biomater. 136 (2021) 570–581, doi:10.1016/j.actbio.2021.09.027.
[41] G. Neag, M. Finlay, A.J. Naylor, The cellular choreography of osteoblast angiotropism in bone development and homeostasis, Int. J. Mol. Sci. 22 (2021), doi:10.3390/ijms22147253.
[42] A. Thiel, M.K. Reumann, A. Boskey, J. Wischmann, R. von Eisenhart-Rothe, P. Mayer-Kuckuk, Osteoblast migration in vertebrate bone, Biol. Rev. 93 (2018) 350–363, doi:10.1111/brv.12345.
[43] V. Kartsogiannis, K.W. Ng, Cell lines and primary cell cultures in the study of bone cell biology, Mol. Cell. Endocrinol. 228 (2004) 79–102, doi:10.1016/j.mce.2003.06.002.
[44] K. Fritton, P.G. Ren, E. Gibon, A.J. Rao, T. Ma, S. Biswal, S.S. Gambhir, S.B. Goodman, Exogenous MC3T3 preosteoblasts migrate systemically and mitigate the adverse effects of wear particles, Tissue Eng. Part A 18 (2012) 2559–2567, doi:10.1089/ten.TEA.2012.0086.
[45] M. Vallet-Regi, A. Rámila, R.P. del Real, J. Pérez-Pariente, A new property of MCM-41: drug delivery system, Chem. Mater. 13 (2001) 308–311, doi:10.1021/cm0011559.
[46] M. Manzano, M. Vallet-Regí, Mesoporous silica nanoparticles for drug delivery, Adv. Funct. Mater. 30 (2020) 1902634, doi:10.1002/adfm.201902634.
[47] T.I. Janjua, Y. Cao, C. Yu, A. Popat, Clinical translation of silica nanoparticles, Nat. Rev. Mater. 6 (2021) 1072–1074, doi:10.1038/s41578-021-00385-x.
[48] Z. Li, Y. Zhang, N. Feng, Mesoporous silica nanoparticles: synthesis, classification, drug loading, pharmacokinetics, biocompatibility, and application in drug delivery, Expert Opin. Drug Deliv. 16 (2019) 219–237, doi:10.1080/17425247.2019.1575806.
[49] P. Kazemzadeh, K. Sayadi, A. Toolabi, J. Sayadi, M. Zeraati, N.P.S. Chauhan, G. Sargazi, Structure-property relationship for different mesoporous silica nanoparticles and its drug delivery applications: a review, Front. Chem. 10 (2022) 823785, doi:10.3389/fchem.2022.823785.
[50] Q. Cai, Z.S. Luo, W.Q. Pang, Y.W. Fan, X.H. Chen, F.Z. Cui, Dilute solution routes to various controllable morphologies of MCM-41 silica with a basic medium, Chem. Mater. 13 (2001) 258–263, doi:10.1021/cm990661z.
[51] S. Brunauer, P.H. Emmett, E. Teller, Adsorption of gases in multimolecular layers, J. Am. Chem. Soc. 60 (1938) 309–319, doi:10.1021/ja01269a023.
[52] E.P. Barrett, L.G. Joyner, P.P. Halenda, The determination of pore volume and area distributions in porous substances. I. Computations from nitrogen isotherms, J. Am. Chem. Soc. 73 (1951) 373–380, doi:10.1021/ja01145a126.
[53] D.A. Kurdyukov, D.A. Eurov, D.A. Kirilenko, V.V Sokolov, V.G. Golubev, Tailoring the size and microporosity of Stöber silica particles, Microporous Mesoporous Mater. 258 (2018) 205–210, doi:10.1016/j.micromeso.2017.09.017.
[54] M. Manzano, V. Aina, C.O. Areán, F. Balas, V. Cauda, M. Colilla, M.R. Delgado, M. Vallet-Regí, Studies on MCM-41 mesoporous silica for drug delivery: effect of particle morphology and amine functionalization, Chem. Eng. J. 137 (2008) 30–37, doi:10.1016/j.cej.2007.07.078.
[55] X. Dai, F. Qiu, X. Zhou, Y. Long, W. Li, Y. Tu, Amino-functionalized MCM-41 for the simultaneous electrochemical determination of trace lead and cadmium, Electrochim. Acta 144 (2014) 161–167, doi:10.1016/j.electacta.2014.08.093.
[56] O.V Bondar, D.V Saifullina, I.I. Shakhmaeva, I.I. Mavlyutova, T.I. Abdullin, Monitoring of the zeta potential of human cells upon reduction in their viability and interaction with polymers, Acta Nat. 4 (2012) 78–81 https://pubmed.ncbi.nlm.nih.gov/22708066.
[57] A. Disalvo, M.A. Frias, Surface characterization of lipid biomimetic systems, Membranes 11 (2021) (Basel), doi:10.3390/membranes11110821.
[58] A. Noureddine, A. Maestas-Olguin, E.A. Saada, A.E. LaBauve, J.O. Agola, K.E. Baty, T. Howard, J.K. Sabo, C.R.S. Espinoza, J.A. Doudna, J.S. Schoeniger, K.S. Butler, O.A. Negrete, C.J. Brinker, R.E. Serda, Engineering of monosized lipid-coated mesoporous silica nanoparticles for CRISPR delivery, Acta Biomater. 114 (2020) 358–368, doi:10.1016/j.actbio.2020.07.027.
[59] J. Yoon, W. Jo, D. Jeong, J. Kim, H. Jeong, J. Park, Generation of nanovesicles with sliced cellular membrane fragments for exogenous material delivery, Biomaterials 59 (2015) 12–20, doi:10.1016/j.biomaterials.2015.04.028.
[60] L. Liu, X. Bai, M.V. Martikainen, A. Kårlund, M. Roponen, W. Xu, G. Hu, E. Tasciotti, V.P. Lehto, Cell membrane coating integrity affects the internalization mechanism of biomimetic nanoparticles, Nat. Commun. 12 (2021) 5726, doi:10.1038/s41467-021-26052-x.
[61] L.D. Quarles, D.A. Yohay, L.W. Lever, R. Caton, R.J. Wenstrup, Distinct proliferative and differentiated stages of murine MC3T3-E1 cells in culture: An *in vitro* model of osteoblast development, J. Bone Miner. Res. 7 (1992) 683–692, doi:10.1002/jbmr.5650070613.
[62] Z. Yu, Q. Li, J. Wang, Y. Yu, Y. Wang, Q. Zhou, P. Li, Reactive oxygen species-related nanoparticle toxicity in the biomedical field, Nanoscale Res. Lett. 15 (2020) 115, doi:10.1186/s11671-020-03344-7.
[63] A.Y. Andreyev, Y.E. Kushnareva, A.A. Starkov, Mitochondrial metabolism of reactive oxygen species, Biochemistry 70 (2005) 200–214 (Mosc)., doi:10.1007/s10541-005-0102-7.
[64] S.M. Schieke, J.P.J. McCoy, T. Finkel, Coordination of mitochondrial bioenergetics with G1 phase cell cycle progression, Cell Cycle 7 (2008) 1782–1787, doi:10.4161/cc.7.12.6067.